HHS Public Access

Author manuscript

Small. Author manuscript; available in PMC 2017 November 01.

Published in final edited form as:

Small. 2016 November ; 12(41): 5750–5758. doi:10.1002/smll.201601696.

Facile Preparation of Multifunctional WS_2/WO_x Nanodots for Chelator-Free ^{89}Zr-labeling and *In Vivo* PET Imaging

Dr. Liang Cheng[1,2], **Dr. Anyanee Kamkaew**[2], **Mr. Sida Shen**[1], **Mr. Hector F. Valdovinos**[3], **Dr. Haiyan Sun**[2], **Mr. Reinier Hernandez**[2], **Ms. Shreya Goel**[4], **Ms. Teng Liu**[1], **Mr. Cyrus R. Thompson**[2], **Todd E. Barnhart Dr.**[3], **Prof. Zhuang Liu**[1], and **Prof. Weibo Cai**[2,3,4,5]

Zhuang Liu: zliu@suda.edu.cn; Weibo Cai: wcai@uwhealth.org

[1]Institute of Functional Nano & Soft Materials (FUNSOM), Collaborative Innovation Center of Suzhou Nano Science and Technology, Soochow University, Suzhou, Jiangsu 215123, China

[2]Department of Radiology, University of Wisconsin-Madison, Wisconsin 53705, United States

[3]Department of Medical Physics, University of Wisconsin-Madison, Wisconsin 53705, United States

[4]Materials Science Program, University of Wisconsin-Madison, Wisconsin 53705, United States

[5]University of Wisconsin Carbone Cancer Center, Madison, Wisconsin 53705, United States

Abstract

While position emission tomography (PET) is an important molecular imaging technique for both preclinical research and clinical disease diagnosis/prognosis, chelator-free radiolabeling has emerged as a promising alternative approach to label biomolecules or nanoprobes in a facile way. Herein, starting from bottom-up synthesized WS_2 nanoflakes, we fabricate a unique type of WS_2/WO_x nanodots, which could function as inherent hard oxygen donor for stable radio-labeling with Zirconium-89 isotope (^{89}Zr). Upon simply mixing, ^{89}Zr can be anchored on the surface of polyethylene glycol (PEG) modified WS_2/WO_x (WS_2/WO_x-PEG) nanodots via a chelator-free method with surprisingly high labeling yield and great stability. A higher degree of oxidation in the WS_2/WO_x-PEG sample (WS_2/WO_x (0.4)) produces more electron pairs, which would be beneficial for chelator-free labeling of ^{89}Zr with higher yields, suggesting the importance of surface chemistry and particle composition to the efficiency of chelator-free radiolabeling. Such ^{89}Zr-WS_2/WO_x (0.4)-PEG nanodots are found to be an excellent PET contrast agent for *in vivo* imaging of tumors upon intravenous administration, or mapping of draining lymph nodes after local injection.

Graphical Abstract

Correspondence to: Zhuang Liu, zliu@suda.edu.cn; Weibo Cai, wcai@uwhealth.org.

Supporting Information

Supporting Information is available online from the Wiley Online Library or from the author.

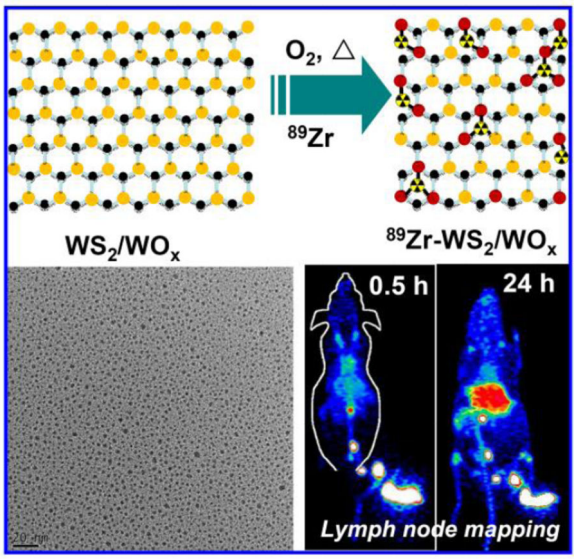

Ultra-small WS_2/WO_x nanodots are fabricated and used as inherent hard oxygen donors for stable radio-labeling with Zirconium-89 (^{89}Zr). Such ^{89}Zr-WS_2/WO_x-PEG nanodots are found to be an excellent PET contrast agent for *in vivo* imaging of tumors upon intravenous administration, or mapping of deep-seated draining lymph node network after local injection.

Keywords

WS_2/WO_x nanodots; ^{89}Zr-Chelator-free; Stability; In vivo PET imaging; Lymph node imaging

Introduction

Molecular imaging accelerates translational preclinical research to clinical uses by providing physiological, anatomic, and metabolic information through interrogating certain targets.[1] Among various imaging technologies, positron emission tomography (PET) is a noninvasive, highly sensitive imaging modality suitable for whole body imaging.[2] In addition to the extensive applications of PET as a molecular imaging technique for diagnosis and prognosis of diseases such as cancers, radiolabeling of nanoparticles for PET imaging has also been widely explored not only to track the *in vivo* translocation of nanoparticles, but also to develop unique nanoprobes for imaging of specific targets of interests.[3] To label biomolecules or nanoparticles, chelator molecules such as NOTA (1,4,7-triazacyclononane-1,4,7-triacetic acid) or DOTA (1,4,7,10-tetraazacyclododecane-1,4,7,10-tetraaceticacid) are often conjugated to their surface to allow chelation of radioisotope ions such as copper-64 ($^{64}Cu^{2+}$). Such a strategy has been applied for radioactive labeling of various types of nano-agents such as carbon nanotubes,[4] quantum dots,[5] superparamagnetic iron oxide nanoparticles (SPIONs),[6] and porous silica nanoparticles to enable PET imaging.[7]

However, chelator-based radiolabeling has several well-known limitations.[8] For example, the coordination chemistry of different isotopes varies greatly and there is no molecular

chelator that can effectively bind many radioisotopes interchangeably. Secondly, even isotopes are stably chelated during radiolabeling, transchelation with endogenous proteins or detachment of the surface-bound molecular chelators can strip the nanoparticles of their radiolabels, yielding images that do not reflect the real biodistribution information of those nanoparticles or biomolecules. Thirdly, the introduction of new groups of chelators also would affect the surface properties of molecules or nanoparticles. Recently, chelator-free radiolabeling has emerged as a promising alternative approach to label nanoparticles in a facile way.[8b] By using this strategy, the labeled nanoparticles can preserve their surface coating chemistry as well as native pharmacokinetic profiles, and in the meantime leaving their surface functional groups intact for further modification or bioconjugation. While chelator-free radiolabeling of several different types of nanoparticles have been reported in the recent few years,[8a, 9] how to precisely control the surface chemistry/composition of nanoparticles to achieve the optimal radiolabeling has been relatively less explored to our best knowledge.

Recently, transition-metal dichalcogenides (TMDCs) such as MoS_2, $MoSe_2$, WS_2 and WSe_2 with two-dimensional (2D) structures have emerged as a unique type of functional nanomaterials attractive in many different fields including biomedicine.[10] TMDC nanosheets and their doped or composite nanostructures have shown great promises in nanomedicine for potential applications in biological sensing,[11] multimodal imaging,[12] drug delivery systems,[9c] cancer therapy,[10d, 12a] and tissue engineering.[13] It was also found that radioisotope ions such as $^{64}Cu^{2+}$ could be firmly adsorbed on the surface of MoS_2 nanosheets without the need of chelating molecules, to enable *in vivo* PET imaging.[14]

Compared to TMDC nanosheets, ultra-small dots of TMDCs have larger specific surface area with more edge atoms, and their photoluminescence properties are also interesting for optical imaging and detection.[15] In a few latest studies, MoS_2 and WS_2 dots were prepared by high-powered ultrasonication or high temperature hydrothermal processes,[15a, 15b, 16] during which the Mo (W) edge on the surface of the $Mo(W)S_2$ nanosheets were slightly oxidized.[15a, 17] In this work, we for the first time report that the synthesized WS_2/WO_x nanodots could function as inherent hard oxygen donors for stable radiolabeling of ^{89}Zr, which has a relatively long decay half-life ($t_{1/2}$ = 78.4 h) and a low positron energy (β^+ avg = 395.5 keV) particularly suitable for long-term tracking with PET imaging.[18] Those WS_2/WO_x nanodots with uniform ultra-small sizes but varied oxidation levels are prepared through solution treatment of WS_2 nanoflakes synthesized by a bottom-up method. After functionalization with polyethylene glycol (PEG), the obtained WS_2/WO_x-PEG nanodots can be labeled with ^{89}Zr via a chelator-free method upon simply mixing, yielding ^{89}Zr-WS_2/WO_x-PEG with great labeling yield and high serum/ *in vivo* stability. Importantly, a higher degree of oxidation in the WS_2/WO_x-PEG sample produces more electron pairs, which would be beneficial for chelator-free labeling of ^{89}Zr with higher yields, suggesting the importance of surface chemistry and particle composition to the efficiency of chelator-free radiolabeling. Interestingly, such ^{89}Zr-WS_2/WO_x-PEG nanodots appears to be a great PET imaging probe not only for tumor imaging, but also for *in vivo* mapping of draining lymph nodes, after systemic or local injections, respectively.

Results and discussion

Ultra-small WS_2/WO_x nanodots were synthesized by a high-temperature solvent-thermal method and then broken in dimethyl sulfoxide (DMSO) under solution treatment to obtain small nanodots (Figure 1a). More detailed synthesis procedure could be found in the Experimental Section. Briefly, WS_2 nanoflakes were obtained after adding sulfur/oleyamine (S/OM) into WCl_6 in oleylamine (OM) and 1-octadecene (ODE) mixed solvent at 300 °C. As-synthesized WS_2 showed flake-like structures with an average layer spacing of ~ 2 nm as observed under transmission electron microscope (TEM) (Figure 1b, **left**, Supporting Figure S1&S2). Under solvent-thermal treatment in DMSO within the air atmosphere, WS_2 nanoflakes were broken into smaller sizes (Figure 1b, right). After treatment for 12 h, small WS_2 dots with uniform size at ~5 nm were obtained as revealed by TEM imaging. X-ray diffraction (XRD) was employed to investigate the crystal phase and purity of the as fabricated nanodots (Figure 1c). The characteristics of hexagonal WS_2 (JCPDS card no. 08-0237) were still observed, indicating that the crystal structure of WS_2 nanodots was preserved during the solution treatment. However, after careful analysis the XRD spectrum of those nanodots, we observed a new peak at $2\theta = 25.85°$, which was attributed to orthorhombic tungsten oxide monohydrate ($WO_x \cdot H_2O$, JCPDs card no. 43-0679).

To further investigate the chemical composition of the products obtained after solvent-thermal treatment, X-ray photoelectron spectroscopy (XPS) analysis of as-made WS_2 nanoflakes and nanodots was performed. As shown in Figure 1d, the peaks located at 33.10 and 35.23 eV could be ascribed to $W4f_{7/2}$ and $W4f_{5/2}$ lines of $W(^{IV})$, while those at 36.07 and 38.30 eV corresponded to $W4f_{5/2}$ and $W4f_{7/2}$ peaks of $W(^{VI})$, the latter of which agreed well with that reported for WO_x.[19] Moreover, we also found S and O signals in the spectra of WS_2 nanodots (Supporting Figure S3). These spectroscopy characterizations unambiguously indicated that the obtained nanostructures should contain the complex of WS_2 and WO_x. Furthermore, with extended reaction time, the black color of the sample gradually changed to brown, indicating the further increase of oxidation degree (Figure 1a, Supporting Figure S4a). The approximate WO_x: WS_2 ratios in the WS_2/WO_x composite-nanostructures were measured to be 0.1 : 1, 0.25 : 1, and 0.4 : 1 prepared with the reaction time of 3 h, 6 h, and 12 h, respectively, as determined by XPS spectra of W_{4f}. We thus named the synthesized samples to be WS_2/WO_x (0.1), WS_2/WO_x (0.25), and WS_2/WO_x (0.4) nanodots.

To understand the mechanism in the transformation of WS_2 nanoflakes into WS_2/WO_x nanodots, we carefully studied several synthesis parameters affecting the formation of nanodots. Interestingly, we found that those WS_2 nanoflakes showed little change under argon protection with the same reaction condition in DMSO, suggesting that the reaction atmosphere played an important role in the formation of WS_2/WO_x nanodots. Only under the air atmosphere condition, WS_2 nanoflakes could be transformed into WS_2/WO_x composite nanodots, suggesting the role of oxygen in this reaction process (Equation 1). In addition, enhancing reaction temperature or increasing reaction time would be beneficial for higher degrees of oxidation.

$$WS_2+O_2 \xrightarrow[\Delta]{} WS_2/WO_x+SO_2 \quad (1)$$

In order to enhance the solubility of those WS_2/WO_x nanodots in physiological solutions, a PEG-grafted amphiphilic polymer (poly(maleic anhydride-alt-1-octadecen, C_{18}PMH-PEG) was coated on the surface of as-prepared WS_2/WO_x nanodots.[20] After PEGylation, the obtained WS_2/WO_x (0.4)-PEG with an average hydrodynamic size at ~15 nm exhibited great stability in various physiological solutions including saline, cell culture medium, and fetal bovine serum (Supporting Figure S5). Moreover, with such biocompatible PEG coating, our WS_2/WO_x (0.4)-PEG showed no significant *in vitro* cytotoxicity to cells even at high concentrations (0.2 mg/mL, Supporting Figure S6). UV-vis-NIR spectra of PEGylated WS_2/WO_x (0.4) nanodots revealed a new peak (~277 nm) in the UV region, while its NIR absorbance was dramatically weakened compared with WS_2 nanoflakes (Figure 1e, Supporting Figure S4b). The photoluminescence (PL) spectra of WS_2/WO_x (0.4) nanodots showed strong emission peaked at 470 nm under the excitation wavelength at 370 nm (Figure 1e, Supporting Figure S7). After 2 h of UV irradiation, WS_2/WO_x (0.4)-PEG nanodots showed excellent photostability (Supporting Figure S8).

According to the special structure of the synthesized WS_2/WO_x nanodots, we hypothesized that abundant WO_x groups (W-O-) on the surface of WS_2/WO_x nanodots may function as inherent hard oxygen donors for stable radio-labeling of ^{89}Zr. ^{89}Zr-oxalate was produced according to our previous procedures.[9d] After mixing ^{89}Zr with water-soluble WS_2/WO_x -PEG nanodots in HEPES buffer (0.5 mM) at pH ~7 under 75 °C, which appeared to be the optimal condition for ^{89}Zr-labeling in this system (Supporting Figure S9), 90% of ^{89}Zr was strongly adsorbed on the WS_2/WO_x (0.4)-PEG nanodots surface after only 15 mins (Figure 2a&b), and the ^{89}Zr labeling yield reached to as high as 95% after 2 h of incubation. In order to obtain accurate labeling yield, ethylenediaminetetraacetic acid (EDTA) and pisothiocyanatobenzyl desferrioxamine B (DFO) were used as simpler and stronger competitive chelation agents for the thin layer chromatography (TLC) analysis to remove any unstable ^{89}Zr loosely associated with those nanodots. Though some weakly bound ^{89}Zr was eliminated from the system, a high labeling yield > 80% was still obtained under the challenge condition (Figure 2a). Furthermore, some negative control experiments with the mixture of free ^{89}Zr and polymer (C_{18}PMH-PEG) showed nearly zero labeling yields, confirming the successful labeling of ^{89}Zr on WS_2/WO_x (0.4)-PEG nanodots.

To understand how the composition of nanoparticles would affect their radiolabeling, WS_2 and WS_2/WO_x nanostructures with different oxidation degrees were labeled with ^{89}Zr using this chelator-free method (Figure 2c). With the oxidation degree enhanced, the labeling yield increased significantly: 81.8 % of WS_2/WO_x (0.4) nanodots > 59.1 % of WS_2/WO_x (0.25) nanodots > 38.5 % of WS_2/WO_x (0.1) nanodots >17.6 % of WS_2 nanoflakes. This phenomenon is likely due to more electron pairs on the surface of WS_2/WO_x (0.4) nanodots than that for other samples. $^{89}Zr^{4+}$ is a hard Lewis acid and thus prefers to bind with hard Lewis bases such as oxygen on WS_2/WO_x (0.4) nanodots that act as electron donors. Notably, we also synthesized WO_3 nanorods following the previous method.[21] However, those WO_3 nanostructures appeared to be rather unstable in aqueous buffers and would be

quickly degraded, thus not suitable for radiolabeling and further imaging applications (Supporting Figure S10). ^{89}Zr labeling on ^{89}Zr-WS_2/WO_x (0.4)-PEG nanodots was also found to be highly stable in mouse serum for up to 72 h even in a DFO competitive situation (Figure 2d, Supporting Figure S11). Therefore, WS_2/WO_x (0.4)-PEG nanodots would be an ideal platform for chelator-free labeling with ^{89}Zr with high labeling yield and excellent stability, promising for *in vivo* PET imaging.

To demonstrate the feasibility of ^{89}Zr-WS_2/WO_x-PEG nanodots for PET imaging and investigate their *in vivo* biodistribution, ^{89}Zr-WS_2/WO_x (0.4)-PEG nanodots solution (200 μL, ~6.5 MBq, dose = 1 mg/kg) was intravenously (*i. v.*) injected into Balb/c mice bearing 4T1 tumors (Figure 3a). Interestingly, ^{89}Zr-WS_2/WO_x (0.4)-PEG nanodots showed efficient tumor accumulation, which showed a time-dependent increase after injection. Quantitative data obtained from region-of-interest (ROI) analysis of these PET images revealed that the tumor uptake of ^{89}Zr-WS_2/WO_x(0.4)-PEG nanodots were determined to be 4.4 ± 0.8, 6.7 ± 1.4, 8.3 ± 1.3, 11.6 ± 1.7, and 13.7 ± 2.2 %ID/g at 3 h, 6 h, 10 h, 24 h, and 48 h post-injection (p. i.), respectively (Figure 3b). Such an efficient passive tumor homing of nanodots could be owing to the enhanced permeability and retention (EPR) effect of 4T1 tumors. High PET signals in the heart even at later time points suggested long blood circulation time of those nanodots, which should be favorable for the EPR-derived tumor uptake of ^{89}Zr-WS_2/WO_x (0.4)-PEG. Those results demonstrated the possibility of using those nanodots as a PET imaging probe for *in vivo* tumor imaging upon systemic administration.

Beyond high tumor uptake, significant accumulation of ^{89}Zr-WS_2/WO_x (0.4)-PEG nanodots was also observed in the liver, in which the radioactive signals peaked at 12 h p. i. (32 ± 3.8 %ID/g), and slightly decreased to 23.8 ± 3.2 % ID/g at 48 h p. i. Radioactivity signals in the bladder at the first time point could likely be due to the small amount of free ^{89}Zr that was not completely removed prior to injection and got concentrated in the bladder after intravenous injection. Biodistribution of WS_2/WO_x (0.4)-PEG nanodots 48 h after injection also showed efficient tumor uptake, together with its retention in reticuloendothelial systems (RES) including liver and spleen (Figure 3c). In marked contrast, free ^{89}Zr exhibited rapid renal clearance and nearly no uptake in the tumor and liver, instead significant bone uptake was observed (Supporting Figure S12&S13). Surprisingly, mice injected with ^{89}Zr-WS_2/WO_x (0.4)-PEG nanodots showed superb *in vivo* stability throughout 2 weeks, with less than 3 %ID/g bone uptake at day 14 p. i. (Supporting Figure S14). Such a difference in biodistribution patterns evidenced that high *in vivo* labeling stability of ^{89}Zr-WS_2/WO_x (0.4)-PEG nanodots. Notably, after intravenous injection with a high dose of cold WS_2/WO_x (0.4)-PEG (40 mg/Kg), which was 40 times of the imaging dose, we did not find any significant toxicity for the treated mice based on H&E staining and standard biochemistry examination (Supporting Figure S15&16).

The metastatic spread of tumor cells is directly or indirectly responsible for more than 90% of cancer deaths[22]. During cancer lymphatic metastasis, sentinel draining lymph nodes connecting with the primary solid tumor are usually the primary target organs of metastasizing cancer cells[23]. Therefore, it is of great importance to identify the exact locations of draining lymph nodes so as to remove those nodes together with the primary

solid tumor during surgery. To realize lymph node mapping in the clinic, colored dyes or carbon black are injected into the solid tumor, whose draining lymph nodes are then labeled with color to facilitate surgical resection. However, the sensitivity of this method is quite limited. Previous studies have shown that nanoparticles ≥ 4 nm tend to rapidly enter the lymphatic capillaries and may be retained within the lymphatic system, resulting in efficient labeling of the vessels and the sentinel lymph nodes[24]. Lastly, several studies have shown that effective lymph node accumulation of nanoparticles does not require the addition of active targeting agents[23, 25]. As a proof-of-concept, we herein demonstrated the possibility of using noninvasive PET imaging with ^{89}Zr-WS_2/WO_x-PEG probe for highly-sensitive *in vivo* lymph node mapping.

Upon local injection with ^{89}Zr-WS_2/WO_x (0.4)-PEG nanodots (~30 μL, 50 μCi) into the right rear footpad of each mouse, serial PET scans were performed for the treated mice (Figure 4a&4b). An extensive draining lymphatic network containing multiple deep-seated lymph nodes was lightened up under PET imaging as early as 0.5 h post injection of ^{89}Zr-WS_2/WO_x (0.4)-PEG. The signals in those lymph nodes remained to be rather strong 24 h after local injection of ^{89}Zr-WS_2/WO_x(0.4)-PEG (green line in the Figure 4a). In marked contrast, after local injection with free ^{89}Zr (~50 μCi in 30 μL PBS), we could only see PET signals in the first draining lymph node at the first time point (0.5 h p.i.). Later on, free ^{89}Zr would gradually diffuse within the mouse body and showed domination uptake by the bone (Figure 4c&4d), similar to the *in vivo* distribution profile of free ^{89}Zr after intravenous injection (Supporting Figure S12). Therefore, free ^{89}Zr is not suitable for lymph node tracking. It is known that while small molecules could diffuse out of lymphatic vessels, nanoparticles with larger sizes may show limited transportation by lymphatic circulation and thus lower lymph node targeting ability.[26] Although various nanoparticles have been investigated for lymph node imaging, many of them are only capable of imaging a few draining lymph nodes nearby the injection sites.[23, 27] Our ^{89}Zr-WS_2/WO_x (0.4)-PEG nanodots with ultra-small sizes thus appeared to be an ideal PET agent for mapping of the draining lymphatic network with deep-seated lymph nodes.

In addition to acting as an effective nano-probe for chelator-free ^{89}Zr-labeling and PET imaging of tumors and lymphatic networks, such WS_2/WO_x nanodots are featured with several other interesting properties promising in nanomedicine: (**i**) This chelator-free radiolabeling strategy with WS_2/WO_x-PEG nanodots can be effectively utilized for other different kinds of isotopes (e.g. $^{64}Cu^{2+}$) with high labeling yield and stability (Supporting Figure S17); (**ii**) As tungsten (W) processes large X-ray absorption coefficient, WS_2/WO_x-PEG nanodots could offer strong contrast under CT imaging (Supporting Figure S18), and may in the meanwhile be used as a radiosensitizer to enhance radiotherapy of cancer;[12b, 16] (**iii**) The functionalities of WS_2/WO_x nanodots could be further enriched by doping with different types of metal ions (*e.g.* Mn^{2+}, Gd^{3+}) to enable other modalities of imaging such as magnetic resonance imaging (MRI);[12b] (**iv**) Further optimizing the surface modification of WS_2/WO_x nanodots may be helpful not only to allow active targeting of specific biomolecules or lesions of interest, but also to realize renal clearance of those ultra-small nanodots.

Conclusion

In summary, we for the first time reported ultra-small WS_2/WO_x nanodots as inherent hard oxygen donors to label radioisotope ^{89}Zr via a chelator-free manner for *in vivo* PET imaging. By a simple solvent-thermal treatment of WS_2 nanoflakes, WS_2/WO_x nanodots with uniform ultra-small sizes were synthesized. After surface PEGylation, the obtained WS_2/WO_x-PEG nanodots could be labeled with ^{89}Zr upon simple mixing with rather high labeling yield and stability. It was further found that a higher degree of oxidation would be beneficial for chelator-free labeling of ^{89}Zr on WS_2/WO_x nanodots. Utilizing ^{89}Zr-WS_2/WO_X-PEG as the nano-probe, *in vivo* PET imaging of tumors was demonstrated upon systemic administration, and *in vivo* mapping of deep-seated lymph nodes network was further realized with local injection of ^{89}Zr-WS_2/WO_X-PEG. Our work here thus presents an interesting type of nano-probe that can be labeled with a number of different radioisotope ions via the chelator-free manner with high efficiency for PET imaging. The performance of this WS_2/WO_x-PEG nano-probe, while has already shown promises for passive targeting / imaging of tumors, as well as mapping of draining lymphatic network, may be further improved by optimization of its surface modification, or tuning of its elementary composition.

Experimental section

Synthesis of WS_2 nanoflakes

A typical synthesis procedure is described as follows[12b, 28]: 1 mmol WCl_6 was added into a mixed solvent of 20 ml of oleylamine (OM) and 10 ml of 1-octadecene (ODE) in a three-necked flask (50 ml) at room temperature. The solution was heated to 150 °C to remove water and oxygen under vigorous magnetic stirring in the presence of nitrogen for protection for ~30 min. Afterwards, the temperature of the solution was rapidly raised to 300 °C and kept there for another 30 min in the nitrogen atmosphere. A sulfur solution prepared by dissolving 2 mmol S powder in 5 ml OM was then injected into the flask at 300 °C within 10 min. The reaction was kept at 300 °C for 30 min. After the solution was cooled down to room temperature, WS_2 nanoflakes were precipitated by adding anhydrous ethanol (~30 mL), collected by centrifugation, and washed repetitively with ethanol.

Synthesis of WO_3 nanorods

To synthesize WO_3 nanorods[21], tungsten ethoxide was decomposed in the presence of a mixture of trioctyl amine and oleic acid at a 1:1 ratio. The mixture was heated to 300 °C under inert atmosphere. The tungsten ethoxide solution was injected quickly into the flask at 300 °C, and kept at this temperature for another 5 min before removing the heating mantle. Immediately after injection, the color of the solution changed to dark blue. WO_3 nanorods were precipitated by adding 15 mL of ethanol. The product was collected by centrifugation, and thoroughly washed with ethanol.

Synthesis of WS_2/WO_X nanodots

WS_2 nanoflakes were first exfoliated to nanosheets by a solvent-thermal method. Typically, 500 mg of WS_2 nanoflakes and 50 mL of DMSO were added in 100 ml serum bottle and

kept under ultrasonication for 1 h to exfoliate WS_2 nanoflakes by sonicator (KQ5200DB) with an output power at 400 W. Then the dispersion was decanted into flask and heated at 140 °C under vigorous stirring for different periods of time. Afterwards, the resulting suspensions were settled for several hours and centrifuged for 5 min at 14800 rpm to remove large aggregates. The light yellow supernatant was WS_2/WO_x nanodots.

Surface modification with C_{18}PMH-PEG

C_{18}PMH-PEG was synthesized following a literature procedure[20]. For the PEGylation of nanodots, a solution of 50 mg C_{18}PMH-PEG polymer in 1 ml water was added into 5 ml stock solution of WS_2/WO_x (0.4) nanodots (5 mg/mL) in DMSO, and the mixture was stirred overnight before it was transferred into 5 ml water. WS_2/WO_x (0.4)-PEG nanodots were obtained after dialyzing the solution for 1 day in a dialysis bag (MWCO 14 kDa) to remove DMSO and other reagents. The resultant solution was centrifuged at speed of 5000 rpm to remove large aggregates (with supernatant collected). Excess PEG molecules were then removed by centrifugation at 14800 rpm (10 min) to collect the precipitate, which was then re-suspended in water for future use.

Characterization

The phase and crystallography of the WS_2 nanoflakes and WS_2/WO_X nanodots were characterized by using a PANalytical X-ray diffractometer equipped with Cuka radiation (λ=0.15406 nm). A scanning rate at 0.05 $°s^{-1}$ was applied to record the pattern in the 2θ range of 10–80°. Transmission electron microscopy (TEM) images of the nanoflakes were obtained using a FEI Tecnai F20 transmission electron microscope equipped with an energy dispersive spectroscope (EDX) at an acceleration voltage of 200 kV. X-ray photoelectron spectra (XPS) was performed on an SSI S-Probe XPS Spectrometer. UV-vis-NIR spectra were obtained with PerkinElmer Lambda 750 UV-vis-NIR spectrophotometer. Fluorescence spectra of different samples were obtained on a FluoroMax 4 luminescence spectrometer (HORIBA Jobin Yvon). The hydrodynamic diameters of WS_2/WO_X-PEG nanodots were determined by a Zetasizer Nano-ZS (Malvern Instruments, UK).

^{89}Zr labeling

^{89}Zr was produced with an onsite cyclotron (GE PETrace) in University of Wisconsin-Madison. $^{89}ZrCl_2$ (150 MBq) was diluted in 300 μL of 1 mM HEPES solution (pH ~ 7) and mixed with 100 μL of WS_2/WO_x (0.4)-PEG nanodots (1 mg/mL). The reaction was conducted at 75 °C for 120 min with constant shaking. The labeling yield was determined by thin-layer chromatography (TLC) at different time points. In order to obtain accurate labeling yield, ethylenediaminetetraacetic acid (EDTA) and p-isothiocyanatobenzyl desferrioxamine B (DFO) were used as simpler and stronger competitive chelation agents in the TLC analysis to remove any unstable ^{89}Zr loosely associated with those nanodots. Before TLC analysis, we added EDTA (0.5 mM, 25 μL) or DFO dissolved in DMSO solution (1 mM, 25 μL) was added into 25 μL ^{89}Zr-WS_2/WO_x (0.4) solution and was shaken for 5 min at each time point. We also investigated the labeling yields under different pH values, temperatures, and different oxygen degrees of WS_2/WO_x nanocomposites. The resulting ^{89}Zr-WS_2/WO_X-PEG was purified by a PD-10 column using PBS as the mobile phase.

Serum stability studies

For serum stability study, ^{89}Zr-WS_2/WO_x (0.4)-PEG nanodots were incubated in complete mouse serum at 37 °C for up to 72 h. Portions of the mixture were sampled at different time points and filtered through 100 kDa cut-off filters. The filtrates were collected and their radioactivities were measured. The percentages of retained (i.e., intact) ^{89}Zr on the WS_2/WO_x (0.4)-PEG nanodots were calculated using the following equation: (total radioactivity - radioactivity in filtrate)/total radioactivity.

DFO Challenge Study

To demonstrate the stability of ^{89}Zr-WS_2/WO_x (0.4) nanodots, DFO with the concentration of 1 mM was added into 250 μL of ^{89}Zr-WS_2/WO_x (0.4)-PEG (~300 μCi) completely mouse serum solution (pH=7) at 37 °C under constant shaking (550 rpm) for 72 h. At each time point, 25 μL of mixture was taken out and resuspended in 100 μL of HEPES. A 300 kDa filter was used to separate potential ^{89}Zr-DFO from ^{89}Zr-labeled nanomaterials. The ^{89}Zr-DFO and ^{89}Zr-WS_2/WO_x (0.4) nanodots radio-activity was measured by using a gamma counter (PerkinElmer).

In vitro toxicity of WS_2/WOx-PEG nanodots

4T1 murine breast cancer cells were cultured in the standard cell medium recommended by American type culture collection (ATCC) under 37 °C within 5% CO_2 atmosphere. Cells seeded into 96-well plates at a density of $1*10^4$ cells per well were incubated with different concentrations of WS_2/WO_x (0.4)-PEG nanodots for 24 h. Relative cell viabilities were determined by the standard methyl thiazolyl tetrazolium (MTT) assay.

Tumor model

All animal studies were conducted under a protocol approved by the University of Wisconsin Institutional Animal Care and Use Committee. The 4T1 tumors were generated by subcutaneous injection of $1*10^6$ cells in ~30μL serum-free RMPI-1640 medium onto the back of each female Balb/c mice. After the tumor volume grown to ~70 mm^3, the mice were chosen for *in vivo* PET imaging.

In vivo PET imaging and biodistribution studies

For PET imaging, 4T1 tumor-bearing mice (3 mice per group) post *i.v.* injection of ~6.5 MBq of ^{89}Zr-WS_2/WO_x (0.4)-PEG (dose = 1 mg/kg) were imaged using a microPET/microCT Inveon rodent model scanner (Siemens Medical Solutions USA, Inc.). Data acquisition, image reconstruction, and ROI analysis of the PET data were performed as described previously[29]. After the last PET scan at 48 h post-injection, biodistribution studies were carried out to confirm that the %ID/g values based on PET imaging would truly represent the radioactivity distribution in mice. For the control experiment, three Balb/C mice were *i. v.* injected with free ^{89}Zr to investigate the imaging and biodistribution. For the investigation of long-term *in vivo* labeling stability, three ICR mice *i. v.* injected with ^{89}Zr-WS_2/WO_x (0.4)-PEG nanodots were used to study the biodistribution at different time points. For *in vivo* lymph node mapping with PET, 30 μL of ^{89}Zr-WS_2/WO_x (0.4)-PEG

(~1.85 MBq) or free ^{89}Zr was injected into the right footpad of mouse. The time points at 0.5, 1, 4, 8, and 24 h post injection were chosen for PET scans.

In vivo toxicity of WS_2/WO_x-PEG nanodots

Healthy Balb/c mice were *i. v.* injected with WS_2/WO_x (0.4)-PEG nanodots (200 μL, 40 mg/kg) and sacrificed at various time points (7 days and 30 days p.i., three mice per time point) after injection. For histological examination, major organs from the treated groups and the control group were fixed in 4% formalin and then conducted with paraffin embedded sections for H&E staining. The slices were examined and observed by a digital microscope (Leica QWin).

Blood analysis

Ten healthy Balb/c mice were *i. v.* injected with WS_2/WO_x (0.4)-PEG (a dose of 40 mg/kg). Other five mice were used as the un-treated control. Mice were sacrificed to collect the blood (0.8 mL) for blood biochemistry assay and complete blood panel test at 1 day and 14 days post injection of WS_2/WO_x (0.4)-PEG. The serum chemistry data and complete blood panel were measured in Shanghai Research Center for Biomodel Organism.

Supplementary Material

Refer to Web version on PubMed Central for supplementary material.

Acknowledgments

This work was supported by the National Natural Science Foundation of China (51525203, 51302180, 51572180), the National “973” Program of China (2012CB932601), a Project Funded by the Priority Academic Program Development of Jiangsu Higher Education Institutions, the Post-doctoral science foundation of China (2013M531400, 2014T70542), the University of Wisconsin-Madison, the National Institutes of Health (NIBIB/NCI 1R01CA169365, P30CA014520, 5T32GM08349), the National Science Foundation (DGE-1256259), and the American Cancer Society (125246-RSG-13-099-01-CCE). L. Cheng also acknowledges the Collaborative Innovation Center of Suzhou Nano Science and Technology (Nano-CIC) for the fellowship of “Young Scientists Overseas Exchanges and Cooperation Program”.

References

1. a Weissleder R, Pittet MJ. Nature. 2008; 452:580. [PubMed: 18385732] b Gambhir SS. Nat. Rev. Cancer. 2002; 2:683. [PubMed: 12209157] c Weber WA, Grosu AL, Czernin J. Nat. Clin. Prac. Oncol. 2008; 5:160.d Sun X, Cai W, Chen X. Acc. Chem. Res. 2015; 48:286. [PubMed: 25635467]
2. Ametamey SM, Honer M, Schubiger PA. Chem. Rev. 2008; 108:1501–1516. [PubMed: 18426240]
3. a Phillips E, Penate-Medina O, Zanzonico PB, Carvajal RD, Mohan P, Ye Y, Humm J, Gönen M, Kalaigian H, Schöder H, Strauss HW, Larson SM, Wiesner U, Bradbury MS. Sci. Transl. Med. 2014; 6:260ra149.b Gao J, Gu H, Xu B. Acc. Chem. Res. 2009; 42:1097. [PubMed: 19476332] c Thorek DLJ, Ulmert D, Diop N-FM, Lupu ME, Doran MG, Huang R, Abou DS, Larson SM, Grimm J. Nat. Commun. 2014; 5d Nahrendorf M, Zhang H, Hembrador S, Panizzi P, Sosnovik DE, Aikawa E, Libby P, Swirski FK, Weissleder R. Circulation. 2008; 117:379. [PubMed: 18158358] e Devaraj NK, Keliher EJ, Thurber GM, Nahrendorf M, Weissleder R. Bioconjugate Chem. 2009; 20:397.
4. Liu Z, Cai W, He L, Nakayama N, Chen K, Sun X, Chen X, Dai H. Nat. Nanotechnol. 2007; 2:47. [PubMed: 18654207]
5. Cai W, Chen K, Li Z-B, Gambhir SS, Chen X. J Nucl. Med. 2007; 48:1862. [PubMed: 17942800]

6. Yang X, Hong H, Grailer JJ, Rowland IJ, Javadi A, Hurley SA, Xiao Y, Yang Y, Zhang Y, Nickles RJ, Cai W, Steeber DA, Gong S. Biomaterials. 2011; 32:4151. [PubMed: 21367450]
7. Chen F, Hong H, Zhang Y, Valdovinos HF, Shi S, Kwon GS, Theuer CP, Barnhart TE, Cai W. ACS Nano. 2013; 7:9027. [PubMed: 24083623]
8. a Zhou M, Zhang R, Huang M, Lu W, Song S, Melancon MP, Tian M, Liang D, Li C. J Am. Chem. Soc. 2010; 132:15351–15358. [PubMed: 20942456] b Shaffer TM, Wall MA, Harmsen S, Longo VA, Drain CM, Kircher MF, Grimm J. Nano Lett. 2015; 15:864. [PubMed: 25559467]
9. a Chen F, Ellison PA, Lewis CM, Hong H, Zhang Y, Shi S, Hernandez R, Meyerand ME, Barnhart TE, Cai W. Angew. Chem. Int. Ed. 2013; 52:13319.b Chakravarty R, Valdovinos HF, Chen F, Lewis CM, Ellison PA, Luo H, Meyerand ME, Nickles RJ, Cai W. Adv. Mater. 2014; 26:5119. [PubMed: 24944166] c Liu T, Wang C, Gu X, Gong H, Cheng L, Shi X, Feng L, Sun B, Liu Z. Adv. Mater. 2014; 26:3433. [PubMed: 24677423] d Chen F, Goel S, Valdovinos HF, Luo H, Hernandez R, Barnhart TE, Cai W. ACS Nano. 2015; 9:7950. [PubMed: 26213260]
10. a Wang QH, Kalantar-Zadeh K, Kis A, Coleman JN, Strano MS. Nat. Nanotechnol. 2012; 7:699. [PubMed: 23132225] b Duan X, Wang C, Pan A, Yu R, Duan X. Chem. Soc. Rev. 2015; 44:8859. [PubMed: 26479493] c Chen Y, Tan C, Zhang H, Wang L. Chem. Soc. Rev. 2015; 44:268.d Yin W, Yan L, Yu J, Tian G, Zhou L, Zheng X, Zhang X, Yong Y, Li J, Gu Z, Zhao Y. ACS Nano. 2014; 8:6922. [PubMed: 24905027]
11. Zhu C, Zeng Z, Li H, Li F, Fan C, Zhang H. J Am. Chem. Soc. 2013; 135:5998. [PubMed: 23570230]
12. a Cheng L, Liu J, Gu X, Gong H, Shi X, Liu T, Wang C, Wang X, Liu G, Xing H, Bu W, Sun B, Liu Z. Adv. Mater. 2014; 26:1886. [PubMed: 24375758] b Cheng L, Yuan C, Shen S, Yi X, Gong H, Yang K, Liu Z. ACS Nano. 2015; 9:11090. [PubMed: 26445029]
13. Wu W, Wang L, Li Y, Zhang F, Lin L, Niu S, Chenet D, Zhang X, Hao Y, Heinz TF, Hone J, Wang ZL. Nature. 2014; 514:470. [PubMed: 25317560]
14. Liu T, Shi S, Liang C, Shen S, Cheng L, Wang C, Song X, Goel S, Barnhart TE, Cai W, Liu Z. ACS Nano. 2015; 9:950. [PubMed: 25562533]
15. a Xu S, Li D, Wu P. Adv. Funct. Mater. 2015; 25:1127.b Lin L, Xu Y, Zhang S, Ross IM, Ong ACM, Allwood DA. ACS Nano. 2013; 7:8214. [PubMed: 23968363] c Wang Y, Ni Y. Anal. Chem. 2014; 86:7463. [PubMed: 25001878] d Ha HD, Han DJ, Choi JS, Park M, Seo TS. Small. 2014; 10:3814.
16. Yong Y, Cheng X, Bao T, Zu M, Yan L, Yin W, Ge C, Wang D, Gu Z, Zhao Y. ACS Nano. 2015; 9:12451. [PubMed: 26495962]
17. Zhou P, Xu Q, Li H, Wang Y, Yan B, Zhou Y, Chen J, Zhang J, Wang K. Angew. Chem. Int. Ed. 2015; 54:15226.
18. Holland JP, Divilov V, Bander NH, Smith-Jones PM, Larson SM, Lewis JS. J Nucl. Med. 2010; 51:1293. [PubMed: 20660376]
19. Epifani M, Comini E, Díaz R, Andreu T, Genç A, Arbiol J, Siciliano P, Faglia G, Morante JR. ACS Applied Mater. Interfaces. 2014; 6:16808.
20. Cheng L, He W, Gong H, Wang C, Chen Q, Cheng Z, Liu Z. Adv. Funct. Mater. 2013; 23:5893.
21. Yella A, Tahir MN, Meuer S, Zentel R, Berger R, Panthöfer M, Tremel W. J Am. Chem. Soc. 2009; 131:17566. [PubMed: 19950992]
22. Mehlen P, Puisieux A. Nat. Rev. Cancer. 2006; 6:449. [PubMed: 16723991]
23. Kim S, Lim YT, Soltesz EG, De Grand AM, Lee J, Nakayama A, Parker JA, Mihaljevic T, Laurence RG, Dor DM, Cohn LH, Bawendi MG, Frangioni JV. Nat. Biotechnol. 2004; 22:93. [PubMed: 14661026]
24. a Kobayashi H, Kawamoto S, Bernardo M, Brechbiel MW, Knopp MV, Choyke PL. J Control. Release. 2006; 111:343. [PubMed: 16490277] b Kobayashi H, Kawamoto S, Sakai Y, Choyke PL, Star RA, Brechbiel MW, Sato N, Tagaya Y, Morris JC, Waldmann TA. J Natl. Cancer Institute. 2004; 96:703.
25. a Harisinghani MG, Barentsz J, Hahn PF, Deserno WM, Tabatabaei S, van de Kaa CH, de la Rosette J, Weissleder R. New Eng. J. Med. 2003; 348:2491. [PubMed: 12815134] b Cheng L, Yang K, Li Y, Chen J, Wang C, Shao M, Lee S-T, Liu Z. Angew. Chem. Int. Ed. 2011; 50:7385.

26. Tang L, Yang X, Dobrucki LW, Chaudhury I, Yin Q, Yao C, Lezmi S, Helferich WG, Fan TM, Cheng J. Angew. Chem. Inter. Ed. 2012; 51:12721.

27. a Kobayashi H, Hama Y, Koyama Y, Barrett T, Regino CAS, Urano Y, Choyke PL. Nano Lett. 2007; 7:1711. [PubMed: 17530812] b Torabi M, Aquino SL, Harisinghani MG. J Nucl. Med. 2004; 45:1509. [PubMed: 15347718]

28. Cheng L, Huang W, Gong Q, Liu C, Liu Z, Li Y, Dai H. Angew. Chem. Int. Ed. 2014; 53:7860.

29. Cheng L, Shen S, Shi S, Yi Y, Wang X, Song G, Yang K, Liu G, Barnhart TE, Cai W, Liu Z. Adv. Funct. Mater. 2016; 26:2185. [PubMed: 27110230]

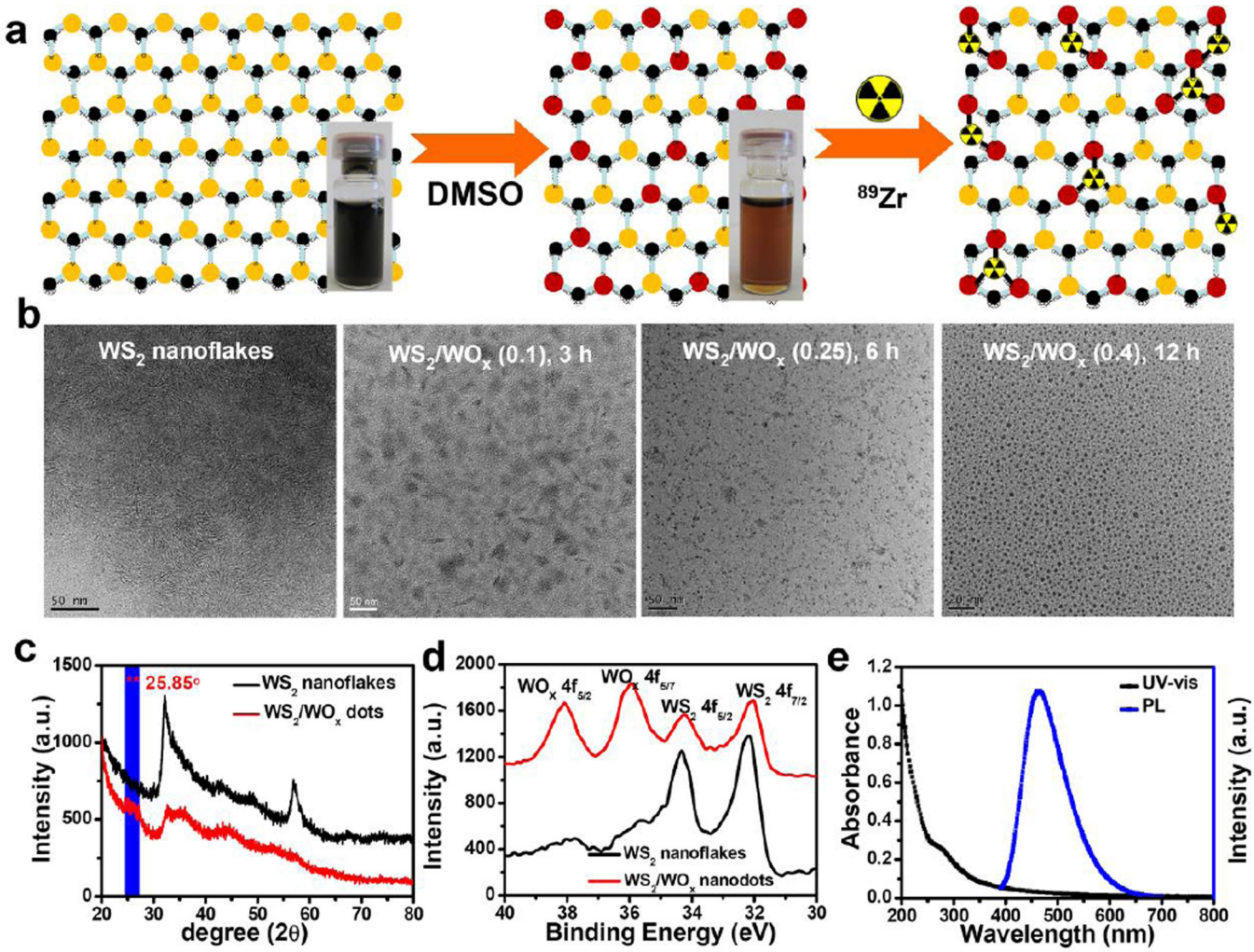

Figure 1.

WS_2/WO_x nanodots synthesis and characterization. **a**) A schematic illustration of WS_2/WO_x nanodots synthesis and ^{89}Zr chelator-free labeling. Inset: Photos of WS_2 nanoflakes after ultrasonication in water (left) and WS_2/WO_x nanodots after solvent-thermal treatment in water (middle). **b**) TEM image of WS_2 nanoflakes (left) and WS_2/WOx nanodots (right) synthesized with different treatment time (3 h, 6 h, and 12 h). **c**) Powder XRD patterns of WS_2 nanoflakes and WS_2/WO_x nanostructures. **d**) High-resolution XPS of as-obtained WS_2 nanoflakes and WS_2/WO_x (0.4) nanodots at binding energies corresponding to W_{4f}. **e**) UV-vis-NIR absorbance and photoluminescence emission spectra of WS_2/WO_x (0.4)-PEG nanodots in water.

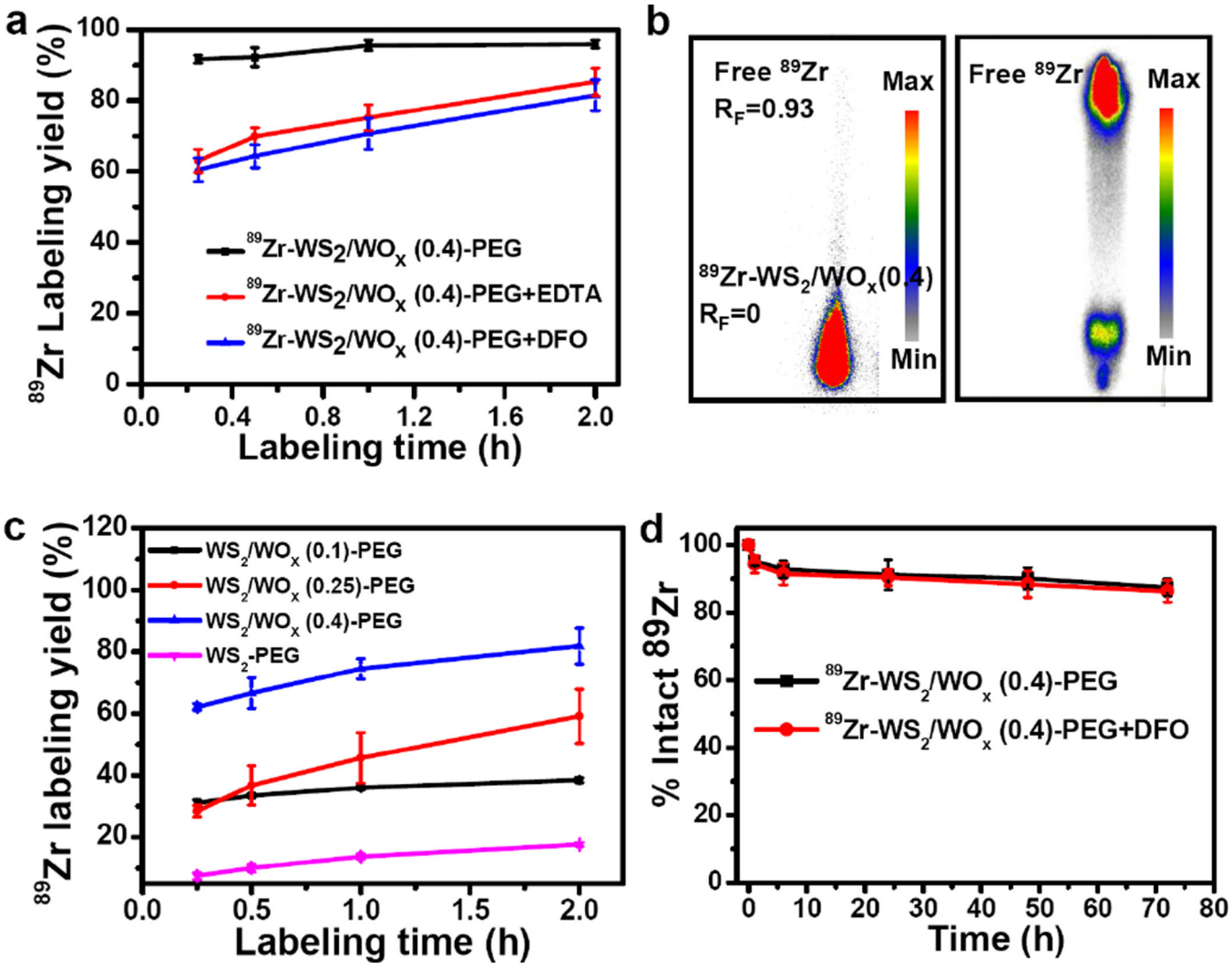

Figure 2.

^{89}Zr chelator-free labeling. **a**) Time-dependent ^{89}Zr labeling yields of WS$_2$/WO$_x$ (0.4)-PEG nanodots without / with EDTA or DFO competitive reaction. **b**) Autoradiograph of TLC plates of ^{89}Zr-WS$_2$/WO$_x$ (0.4)-PEG nanodots (left) and free ^{89}Zr (right). **c**) Time-dependent ^{89}Zr labeling yields of WS$_2$-PEG and different WS$_2$/WO$_x$-PEG nanodots (WS$_2$/WO$_x$ (0.1), WS$_2$/WO$_x$ (0.25), and WS$_2$/WO$_x$ (0.4)) with EDTA competitive reaction. **d**) Serum stability study of ^{89}Zr-WS$_2$/WO$_x$ (0.4)-PEG nanodots incubated in whole mouse serum without or with DFO competitive reaction at 37 °C.

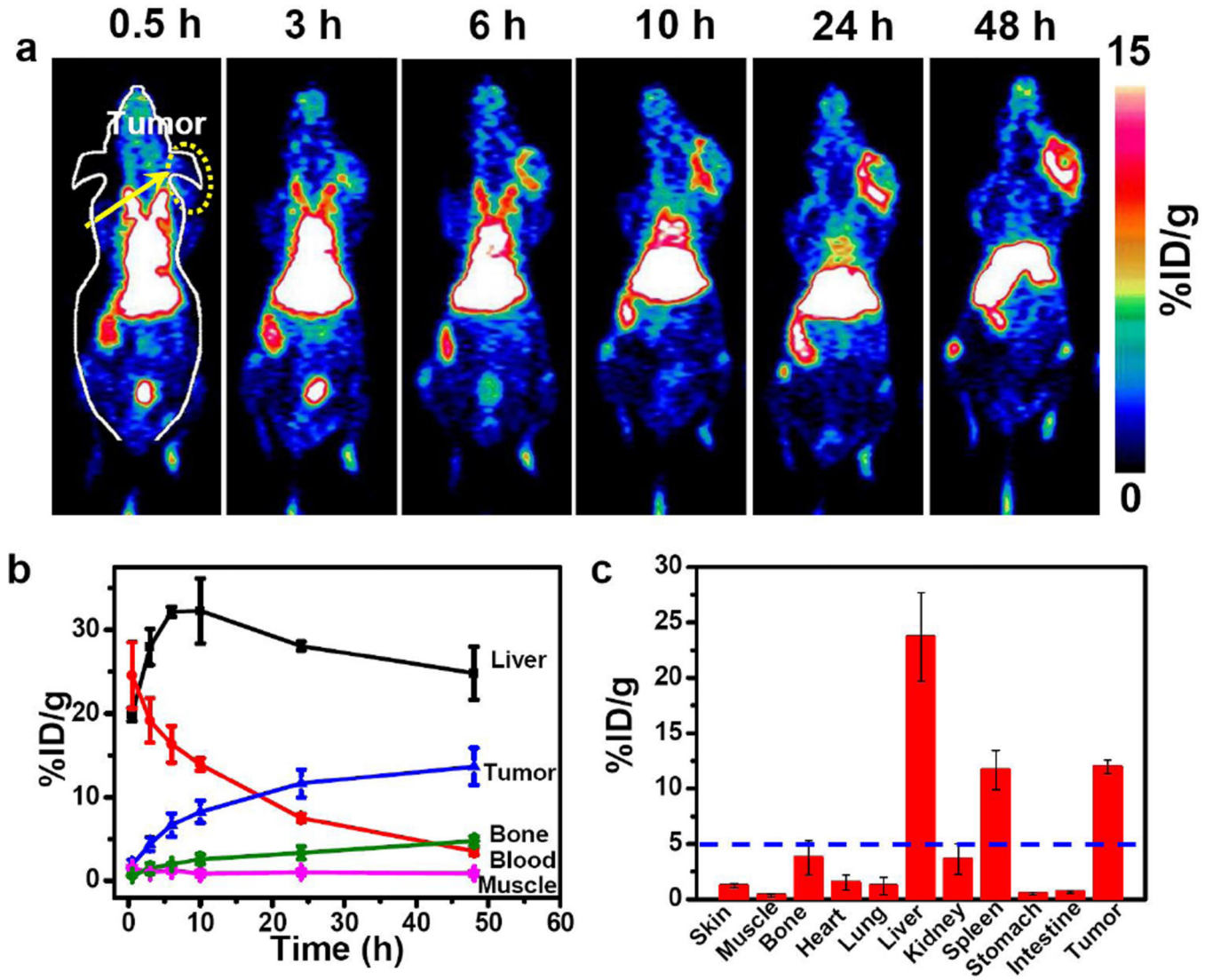

Figure 3.

In vivo tumor imaging after systemic injection. **a)** *In vivo* PET images of 4T1 tumor-bearing mice taken at various time points (0.5, 3, 6, 10, 24, and, 48 h) post intravenous injection of ^{89}Zr-WS_2/WO_x (0.4)-PEG nanodots. (**b**) Quantification of ^{89}Zr-WS_2/WO_x (0.4)-PEG uptake in the liver, tumor, blood, bone, and muscle at various time points p. i. The unit is the percentage of injected dose per gram of tissue (%ID/g). **c**) Biodistribution of ^{89}Zr-WS_2/WO_x (0.4)-PEG nanodots 48 h after intravenous injection into 4T1 tumor-bearing mice as determined by ^{89}Zr radioactivity measurement in various organs (Bl: blood; Sk: Skin; Mu: Muscle; B: Bone; H: Heart;, Lu: Lung; L: Liver; K: Kidney; Sp: Spleen; Pa: Pancreas; St: Stomach; In: Intestine; T: Tumor; Ta: Tail; and Br: Brain). Error bars were based on the standard error of the mean (SEM) of quadruplicate samples.

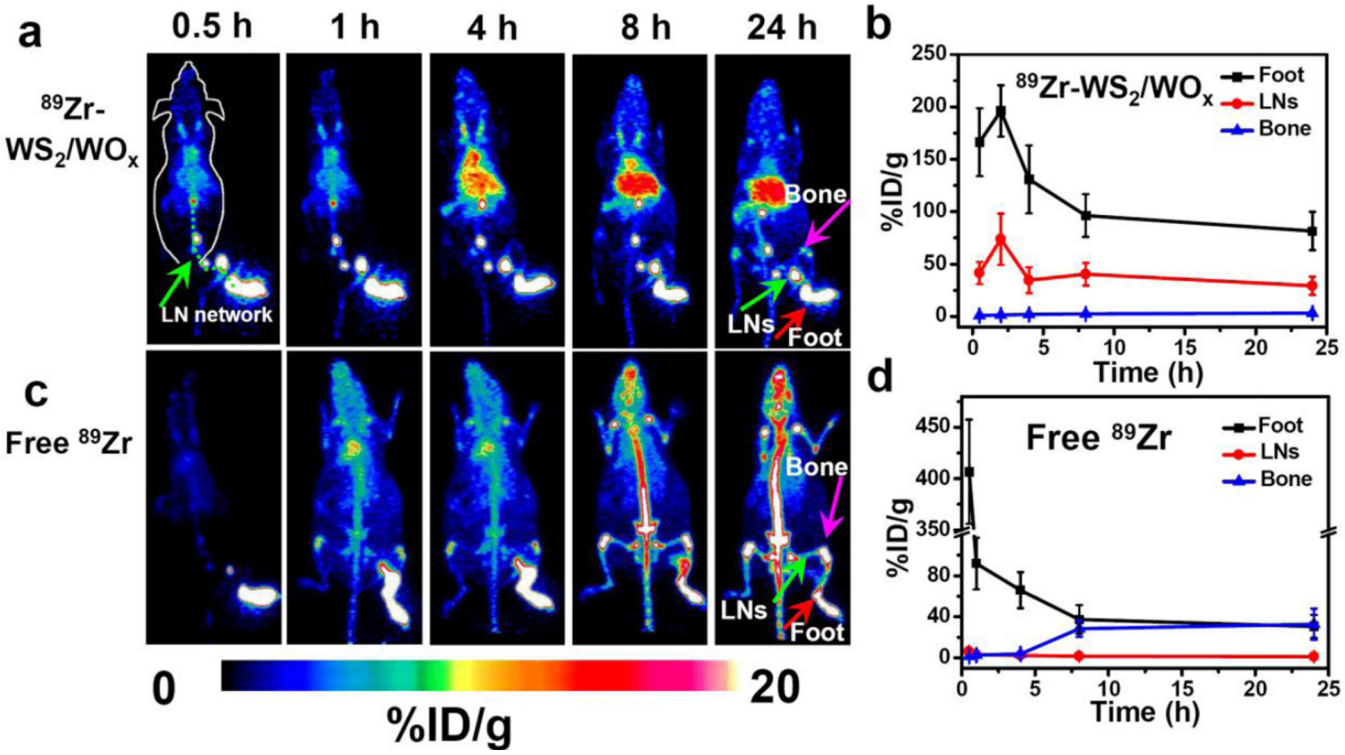

Figure 4.

In vivo lymph node mapping after local injection. **a&c**) *In vivo* lymph node imaging with PET after local injection of ^{89}Zr-WS_2/WO_x (0.4)-PEG nanodots (**a**) and free ^{89}Zr (**c**) into the right footpad of the mouse at different time points. **b&d**) Quantification of ^{89}Zr-WS_2/WO_x (0.4)-PEG nanodots (**b**) and free ^{89}Zr (**d**) uptake by the mouse foot palm, lymph nodes (LNs), and bone.